Controlling homogeneity of the first lithiation in methylated amorphous silicon

Yue Feng, Abdelhak Cheriet, Marianthi Panagopoulou, Damien Aureau, Alistair C.H. Rowe, Catherine Henry-De-Villeneuve, Michel Rosso, François Ozanam

Controlling homogeneity of the first lithiation in methylated amorphous silicon

Yue Feng,[a] Abdelhak Cheriet,[a, b, c] Marianthi Panagopoulou,[a] Damien Aureau,[d] Alistair C. H. Rowe,[a] Catherine Henry-de-Villeneuve,[a] Michel Rosso,[a] François Ozanam[a, *]

a) Laboratoire de Physique de la Matière Condensée, Ecole Polytechnique, CNRS, Institut Polytechnique de Paris, 91120 Palaiseau, France
b) CRTSE, Division Couches Minces Surfaces et Interfaces, 2 Bd Franz Fanon, BP 140 Alger 7-Merveilles 16038, Algeria
c) Faculty of sciences, Farhat Abbas University, Sétif 19000, Algeria
d) Institut Lavoisier, Université de Versailles Saint Quentin en Yvelines, CNRS, Université Paris-Saclay, Versailles, France

Keywords: Li-ion batteries, amorphous silicon, methylated amorphous silicon, lithiation mechanism, operando optical microscopy

Methylated amorphous silicon (a-$Si_{1-x}(CH_3)_x$:H) exhibits a longer life time as an anode material in Li-ion batteries as compared to pure amorphous silicon (a-Si:H). However, operando optical microscopy of thin-film electrodes shows that the first lithiation turns from spatially uniform to non-uniform by increasing the methyl content of the material. The non-uniform lithiation appears to result from an electrostatic instability related to the large resistivity of methylated amorphous silicon. Lithiation spots nucleate either instantaneously at the beginning of the lithiation through dielectric breakdown, or more progressively at morphological defects where the thickness of the layer is reduced. In either case, a damage is generated by the high current density flowing through the locations at which lithiation spots nucleate. Boron doping of methylated amorphous silicon, which decreases the material resistivity, turns the lithiation of thin-film electrodes from non-homogeneous to homogeneous.

1. Introduction

Silicon-based materials exhibit a high capacity for Li incorporation, through alloy formation and have therefore been recognized as promising materials for negative electrodes of lithium-ion batteries. [1, 2] However, silicon is a stiff material with limited elasticity: it cannot sustain the huge deformation – over 300% at full Li loading – associated with massive Li incorporation. [3] The stability of silicon-based anodes during electrochemical lithiation/delithiation cycles

turns out to be very poor, precluding the use of the material in real systems, except in relatively small amounts yielding a corresponding limited gain in capacity. [4] To get rid of such limitations, several approaches have been worked out, mostly based on material nanostructuration since Si nanostructures can afford large deformation much better than larger structures. [5] The need to control the nature of the surface in order to limit the irreversible Solid Electrolyte Interphase (SEI) formation required the design of sophisticated nanostructures (hybrid nanowires, yolk-shell nanostructures, etc.). [6-14] Such an approach has given impressive results in terms of improvement of the cycling capabilities, but remains demanding in terms of synthesis, something which prevents easy upscaling to commercial applications. Progress in electrolyte formulation and alternative binders for composite electrodes also represent significant advances. [15]

An alternative approach (which could be complementary) consists in acting on the material itself. Amorphous silicon has been suggested as a possible alternative to crystalline Si. [16, 17] However, the material stiffness is still too large, and only very thin layers (with therefore a limited areal capacity for Li incorporation) can sustain a large number of lithiation/delithiation cycles. [18-20] The performance of pure and doped or reactive silicon thin-film anodes have recently been reviewed [21, 22]. The comparison between various electrodes is somewhat complex, since the thin-film performances depend on the nature of the substrate, its roughness, the cycling conditions etc. However, a general trend is that thinner films perform better than thicker ones, and that for a given set of test conditions, cracks appear in the thin film above a critical thickness [23, 24]. In this context, a new material, methylated amorphous silicon, has shown a significantly better intrinsic tolerance to electrochemical cycling. [25] Methylated amorphous silicon is a carbon-silicon alloy in which carbon is incorporated under the form of methyl groups. [26] It exhibits a reduced volume density as compared to amorphous silicon and the incorporation of methyl groups (which can only bind to a single Si atom) lowers the

cohesion of the covalent network and makes it mechanically softer than standard amorphous silicon. Moreover, the incorporation of methyl groups does not significantly alter the electronic properties of the material. In particular, the increase of the density of states in the band gap remains limited and the material keeps (to some extent since it becomes much more resistive) its semiconductor properties, [27] which allows for its use as an electrode material. However, despite these improvements, the material is still far from reaching performance levels acceptable for use in commercial systems, and the thickness of the methylated amorphous thin films which can sustain extensive electrochemical cycling does not exceed the 100-nm range. [25]

Therefore, there is a need to better understand the processes associated with lithium incorporation and release in methylated amorphous silicon. This would limit the deleterious effects of the electrochemical cycling and makes the corresponding material amenable to the robustness needed for its use in real systems. [28] In this respect, the first lithiation and delithiation appear to be of prime importance, since this first cycle is the cause of a real dislocation of the material: at the end of the first cycle, the material composition does not change significantly (even if a small proportion of Li remains trapped in the material), but its structure, already amorphous in the pristine state, does. One striking experimental signature of this change can be found in the potential-charge curve of the electrode. This curve exhibits a strong hysteresis at the first cycle, due to the presence of a potential plateau during a large part of the lithiation. This plateau is not seen in the subsequent cycles during which only polarization effects make the potential-charge curves distinct in the lithiation and delithiation phases. [29, 30] Controlling the extent to which the material is disrupted during the first cycle likely has an impact on the long-term stability of the material during electrochemical cycling.

The process according to which the first lithiation takes place in silicon is known to be a two-phase process. [29, 31-34] Lithium is not incorporated progressively into the whole material,

but a strongly lithiated phase forms at the surface, generating stresses which favor the disruption of Si-Si bonds and helping for the progressive penetration of the lithiated phase into the material. [31, 35-38] This behavior is responsible for the existence of the potential plateau during the first lithiation. Using operando optical microscopy, we have recently demonstrated that this behavior takes place homogeneously on pure (device-grade) amorphous silicon (a-Si:H), hereafter termed a-Si, but that it is spatially inhomogeneous on methylated amorphous silicon (a-$Si_{1-x}(CH_3)_x$:H), hereafter termed methylated a-Si (or x% methylated a-Si). This different behavior has tentatively been ascribed to the more resistive character of methylated a-Si and the possible existence of low-resistance defects in the thin-film electrode where lithiation initiates preferentially. [39] The purpose of the present paper is to test this conjecture and find practical means for driving the lithiation homogeneous or non-homogeneous.

2. Experimental

2.1 Preparation of the Amorphous Silicon Electrodes

100 nm-thick a-Si or methylated a-Si (5% or 10% methyl content) thin-films were deposited by radio-frequency Plasma-Enhanced Chemical Vapor Deposition (PECVD) in a low-power regime (plasma power P < 0.3 W cm^{-2}) at 250 ˚C. [26, 27] The pressure during deposition is ~0.05 bar. The flow rate of the silane/methane mixture is kept constant and equal to 33.3 sccm; for a-Si growth, the SiH_4 flow rate is therefore 33.3 sccm; for a-$Si_{0.9}(CH_3)_{0.1}$:H, the SiH_4 flow rate is 13.3 sccm and CH_4 flow rate is 20 sccm; for lower methyl contents, silane and methane flow rates are adjusted as described in Ref. [26]. For boron doping, a supplementary flux of a mixture of 3% B_2H_6 in H_2 was added to the silane/methane mixture. To grow the 1% B-doped material the flow rate of the diborane/dihydrogen mixture was set to 3.9 sccm, and for the 2%B-doped material, it was set to 7.8 sccm. The amount of doping impurity incorporated in the

material was checked using XPS. Despite the poor sensitivity of the XPS detection of boron in silicon, the atomic ratio [B]/[Si] was estimated to be slightly larger than 2% in the 2%B-doped material and consistently slightly larger than 1% in the 1%B-doped material. The density of the deposited material ranges from 2.26 g cm^{-3} (a-Si) to 1.93 g cm^{-3} (10% methylated a-Si). [25] The electronic density of midgap states, determined by current-voltage measurements in the regime of space-charge-limited current (SCLC), is on the order of 5 10^{15} cm^{-3} eV^{-1} in a-Si. [40] It significantly increases when the methyl content exceeds 2% and reaches 10^{17} cm^{-3} eV^{-1} for 5% methylated a-Si and nearly 10^{18} cm^{-3} eV^{-1} for 10% methylated a-Si. [41, 42] Similarly, the resistivity of the material, on the order of 10^{8} Ω cm for a-Si, rises to ~10^{10} Ω cm for 5% methylated a-Si:H and ~10^{12} Ω cm for 10% methylated a-Si, as found from current-voltage measurements in the SCLC regime at various temperatures in a sandwich geometry. [41, 42]. For the 2% B-doped 10% methylated a-Si, the resistivity drops to ~ 10^{7} Ω cm, as found from the linear part of current-voltage measurements performed at room temperature in a planar geometry.

The amorphous Si thin films were deposited on crystalline silicon (c-Si), polished stainless steel (PSS) or non-polished stainless (NPSS) substrates. The c-Si substrates (15 × 15 mm^2) were cut from an n-type Si wafer (resistivity 10-100 Ω.cm, Sil'tronix, France). A gold layer (500 nm thick) was deposited on the back side to ensure an Ohmic contact. Before being introduced into the PECVD chamber, the c-Si substrates were immersed in a 5% HF solution for 15 s to remove the native oxide layer. NPSS substrates (14 × 14 mm^2) were cut from a stainless steel foil (1 mm thick) and subsequently electropolished (3.82 V for 30 min) in a chromosulfuric acid, phosphoric acid, and ethanol mixture [11:55:60 in vol.] at 65˚C to obtain a controlled and reproducible surface state. The PSS surfaces were rinsed in deionized water, deoxidized by exposure to a 5% HF solution for 10 s, rinsed in deionized water again and finally dried under

N_2 flow just prior to their introduction in the PECVD chamber. They were subsequently etched by exposure to H_2 plasma for 10 min before amorphous silicon deposition.

2.2 Electrochemical Experiments

The lithiation/delithiation processes were investigated using home-designed two-electrode half-cells. A cell closed with a glass window was used for operando monitoring the electrode modification by optical microscopy (see Figure 8 in reference [39]). For these experiments, electrodes deposited on PSS substrates were used because light-induced damaging of the electrodes is observed on c-Si substrates. A slightly different cell was used for ex-situ Raman spectroscopy: in a first step lithiation was conducted in the glove box in the dark using the cell shown in **Figure S1**a. Then the stainless-steel cover was replaced by a glass window to keep the electrode under inert argon atmosphere (Figure S1b).

The cells were assembled in an argon-filled glove box (P_{O_2} < 2 ppm, P_{H_2O} < 1 ppm). A lithium-foil (99.9% purity, Sigma-Aldrich) was used as the counter electrode, and 1 M $LiClO_4$ (battery grade, 99.99% purity, Aldrich) in propylene carbonate (PC) (99.7% purity, Sigma-Aldrich) as the electrolyte. All the electrochemical measurements were performed at room temperature (20˚C - 23˚C) using a BioLogic VMP3 multichannel potentiostat or an Autolab PGSTAT12 potentiostat. Lithium charges and discharges were performed by galvanostatic cycling within the 0.025 – 2 V vs. Li/Li^+ potential range for the electrodes deposited on PSS and 0.125 - 2 V for the electrodes deposited on c-Si substrate to avoid lithiation of the underneath Si substrate. Depending on the electrode methyl content, lithiation rates from C/15 to 200 C (full lithiation duration from 15 h down to 18 s) were used, corresponding to current densities in the range 4 - 12600 µA cm^{-2}.

2.3 Optical Microscopy

Operando optical monitoring was performed using a Nikon Optiphot 2 microscope with an objective of 20× magnification (numerical aperture 0.4). The optical images or videos were recorded by a color camera with a field of view of 550 × 345 μm^2 (20× magnification). The same color-range setting was applied to the camera for all experiments, to avoid coloration artefacts due to saturation of any of the RGB channels.

The monitoring of the lithiation was carried out as described elsewhere. [39] The electrode was mounted in the operando cell inside the glove box and the cell was then transferred to the microscope to follow the lithiation process in operando conditions. The images shown in this work were extracted from video recordings of the full lithiation process.

For some experiments, the surface of the a-Si electrodes or of the stainless-steel substrates were characterized by 3D optical confocal microscope Leica DCM8 in confocal mode. An objective of 50× magnification (numerical aperture 0.9) was used. The equivalent pixel size in the image (x/y) is 0.16 µm. The vertical resolution is ≈ 5 nm. The field of view with a 50× magnification objective is 351 × 264 μm^2.

2.4 Raman Spectroscopy and Optical Diffraction Measurements

Raman spectroscopy and optical diffraction measurements were performed using a micro Raman spectrophotometer (LabRAM HR Evolution from HORIBA). A 50× objective was used to focus a blue laser beam (λ = 473 nm, laser spot ≈ 1 μm^2) at the surface of the electrode. Lithiation/delithiation of the electrode were carried out under Ar atmosphere inside the glove box using the cell shown in Figure S1a. After rinsing with propylene carbonate (PC) and dimethyl carbonate (DMC) to remove residual lithium salts and electrolyte from the surface,

the electrode was dried under vacuum and then the cell was again hermetically closed with a glass window (Figure S1b), allowing for its transfer outside the glove box for the Raman characterization. After rinsing and drying, the electrode is stable. No surface evolution was observed as long as the electrode was kept under Ar atmosphere in the closed cell.

3. Results

Before presenting the results, the inhomogeneous lithiation process taking place in methylated a-Si is briefly recalled. A typical example is shown in **Figure 1**. In the early stages of the first lithiation, localized color changes appear on the surface indicating that lithiation does not proceed uniformly but preferentially starts at some locations. With increasing time, the development of circular lithiated areas (lithiation spots) is observed that expand laterally and progressively merge until they invade the entire surface. The observed color changes result from a modification of the optical properties of the active material and an increase of its thickness due to Li insertion. The uniform color at the spot center and the gradual color change on their edges are consistent with their "mesa-like" 3D structure evidenced by AFM characterization. [39] The structural deformations observed by AFM indicate a local thickness increase of ≈ 200%. The constant thickness and uniform color in the center of the spots indicates that the material is fully lithiated in depth with optical properties different from those of the pristine material. In addition, Raman spectroscopy confirms that a change in the material composition is related to the thickness profile: the peaks assigned to amorphous silicon progressively decrease at the spot edge when going from outside to inside the spot (**Figure S2**).

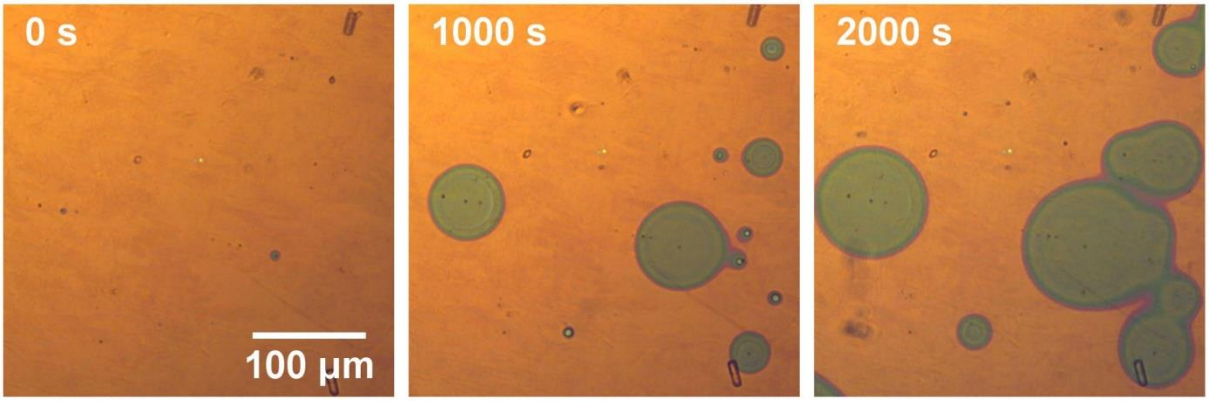

Figure 1. In situ optical images captured during the first lithiation of a 10% methylated a-Si electrode deposited on PSS (100 nm thickness). Green areas are lithiated zones, the brown-orange background is the pristine (non-lithiated) material. The lithiation time is indicated on the images. Lithiation conditions: current density ~ 29 µA cm^{-2} corresponding to a C/2 lithiation rate. The left and right images are those displayed in Figure 4a-b of Reference [39].

Our previous studies had suggested that the high resistivity of the material and the existence of low-resistance point defects might be at the origin of the non-homogeneous lithiation process. [39] Hereafter, we first seek evidence for the existence of such defects. As mentioned in Sec. 2.2, the present work is performed using a $LiClO_4$-PC-based electrolyte in order to be consistent with our previous work. Similar results are found using LP30-FEC-based electrolytes, more representative of the conditions used in actual batteries, as shown in **Figure S3**. This fact is consistent with the mechanisms discussed hereafter, in which electrolyte-dependent features like the nature and properties of the SEI do not come into play.

3.1. Existence of Structural Defects

A first correlation between the nucleation of lithiation spots and the existence of point defects was provided by detailed optical characterizations of the lithiation spots after delithiation. **Figure 2**a shows an optical image of a lithiated area (image of a single lithiation spot). The image was captured after partial lithiation and then delithiation (10% methylated a-Si electrode deposited on a crystalline silicon substrate). The red-pink background outside the circular lithiated area is the pristine silicon layer (non-lithiated area). The color difference between

inside and outside the spot might indicate that a small quantity of lithium remains in the film after delithiation, affecting the refractive index of the layer. The change in the silicon microstructure might also contribute to this effect.

At the center of the spot, a point defect (black dot) is distinguished (zoom in insert). Besides the observation of such defects on the optical image, their presence is further confirmed by illuminating the center of the spots with a laser beam. When the beam is focused at the spot center, a characteristic annular diffraction pattern is systematically obtained (Figure 2b) whereas scattered reflection is observed elsewhere inside the spots (Figure 2c). Such point defects were systematically found at the center of the spots (numerous spots were investigated on the same surface and on different electrodes). An additional piece of information on the nature of the defects is provided by Raman spectroscopy. Raman spectra recorded at the center (red plot) and on area elsewhere in the spot (green plot) are displayed in Figure 2d. In the center, the intensity of the peaks corresponding to the c-Si substrate ($\nu \approx 520$ cm^{-1}, $\nu \approx 900$-1000 cm^{-1}) is stronger and that assigned to the amorphous silicon layer ($\nu \approx 480$ cm^{-1}) is weaker. These observations are consistent with a reduced thickness of the electrode material at the center of the spots.

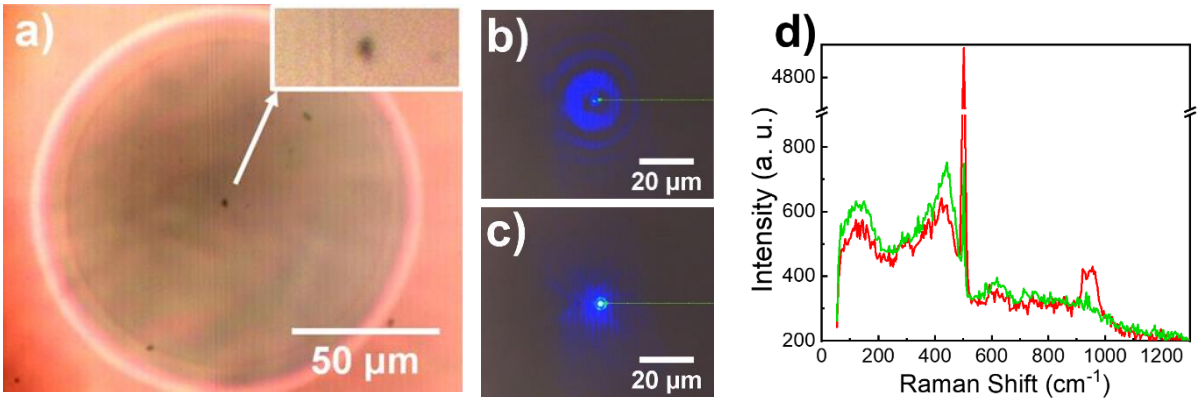

Figure 2. (a) Optical image of a single lithiation spot. The image was captured after partial lithiation (current density ~29 µA cm^{-2}), subsequent delithiation and rinsing with PC and DMC (10% methylated a-Si electrode on PSS, 100 nm thickness). Insert: zoomed image at the spot center highlighting the presence of a point defect (black dot). (b) Annular diffraction pattern and (c) scattered reflection observed at the center of the spot and at nearby areas inside the spot, respectively. The optical patterns were obtained by focusing the laser beam of the Raman

spectrophotometer (λ = 473 nm, 1 μm diameter) at the specified positions. (d) Raman spectra measured at the center of the spot (red plot) and on surrounding area inside the spot (green plot).

Based on these results, the question arises as to whether the defects observed after lithiation/delithiation were pre-existing in the pristine material. The surface of a methylated a-Si electrode was carefully investigated by optical microscopy before lithiation to detect the possible presence of defects and see whether such defects might be preferential lithiation sites. Point defects were identified and their characterization by confocal microscopy indicates that these defects are holes. Some of them are pointed by arrows in **Figure 3**a and the confocal characterization of one of them is shown in Figure 3e-f. Their depth is ≈ 80 nm which is close

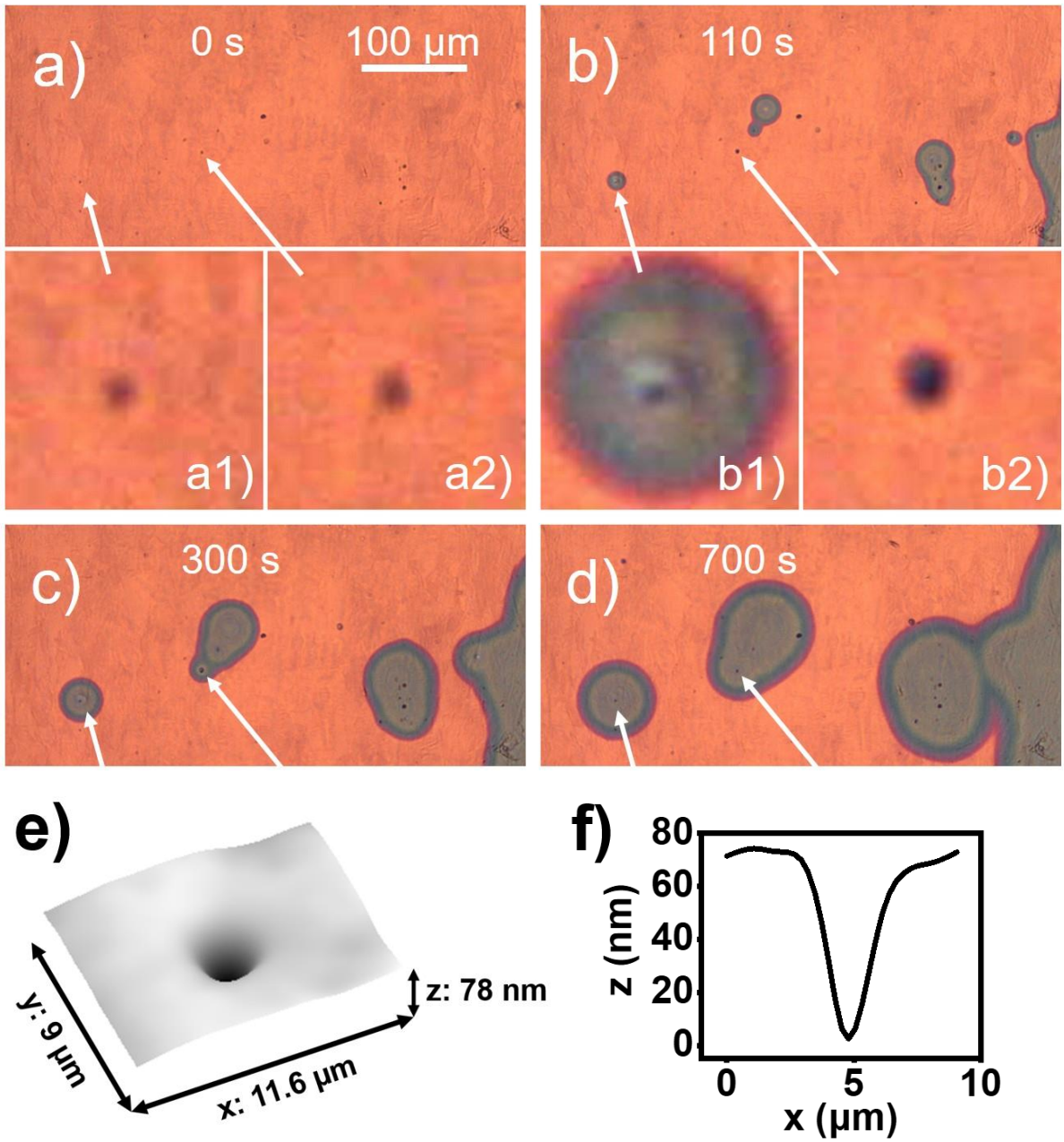

Figure 3. (a-d) Large-field images of a 10% methylated electrode in propylene carbonate + 1 M $LiClO_4$ electrolyte during the first lithiation (operando optical microscopy). (a1, a2, b1, b2) Zoom images showing two specific point defects before and after 110s lithiation. The locations of the defects are pointed with arrows. (e, f) 3D morphology and depth profile of one defect (a1) as measured by confocal microscopy.

to the electrode thickness (100 nm), meaning that on these very localized areas the active material layer is thinner. The surface evolution during lithiation was then specifically monitored on the electrode area where these defects were observed. The sequence of operando optical images of the electrode recorded during lithiation at the same location deserves special interest. Figure 3b-d show some of these images after 110 s (Figure 3b), 300 s (Figure 3c) and 700 s

(Figure 3d) of lithiation time. Zoom images of the two particular defects (labelled 1 and 2) before (images a1 and a2) and after 110s lithiation time (images b1 and b2) are displayed underneath the corresponding large-field images. Their location on the large-field image are indicated by arrows. Other ones have been identified, as shown in **Figure S4**. The image sequence clearly indicates that some of the lithiation spots nucleate at the pre-identified structural defects, other nucleate at locations apparently free of defects, and some pre-identified structural defects do not act as nucleation centers for lithiation spots.

Some spots appear at locations where no structural defect has been pre-identified. This is the case for example of the big spot in the center of the images growing nearby defect 2. Such spots appear at the very beginning of the lithiation, during the potential negative transient [see Figure 2b of Reference [39] and high-magnification images in Figure S4] and their initial growth is very fast (they already have a diameter of 10-15 µm when they first appear in the image sequence). At some pre-identified defects such as defects 1 and 2, lithiation spots appear at a later stage and their initial growth appear slower than that of the very-early-appearing spots. This can be analyzed quantitatively, as shown in **Figure S5**. As a matter of fact, the nucleation of these spots appear time distributed, as revealed in the images shown in Figure 3b-d by the different sizes of the associated spots. Therefore, even if defects do not seem to be the only nucleation sources of lithiation spots, they appear to play a role in this process.

In order to confirm this last statement, the first lithiation was investigated on similar methylated a-Si layer (10% methyl content, 100 nm thick) deposited on different substrates with a variable surface roughness: non-polished stainless steel (NPSS), polished stainless steel (PSS), electronic grade crystalline silicon (c-Si). A comparison of the surface roughness of stainless steel before and after electropolishing is shown in **Figure S6**. Electropolishing removes scratches resulting from metal-foil rolling (vertical dark lines in **Figure 4**a) and significantly reduces the stainless-steel roughness. Nevertheless, the electropolished PSS surfaces remain

much rougher than electronic-grade silicon wafer surfaces. The motivation of this experiment is the hypothesis that a rougher substrate will induce a larger amount of structural defects in the methylated a-Si layer. The three electrodes were partially lithiated using the same conditions (current density ≈ 29 µA cm^{-2} for 12 s). As shown in Figure 4, the density of lithiation spots depends on the electrode substrate. This density is directly correlated to the surface roughness of the substrates on which the methylated a-Si electrodes were deposited (Figure 4d). These results confirm the important (but not exclusive) role played by pre-existing structural defects in the nucleation of lithiation spots. The various possible mechanisms of nucleation of the lithiation spots will be discussed in Section 4.1.

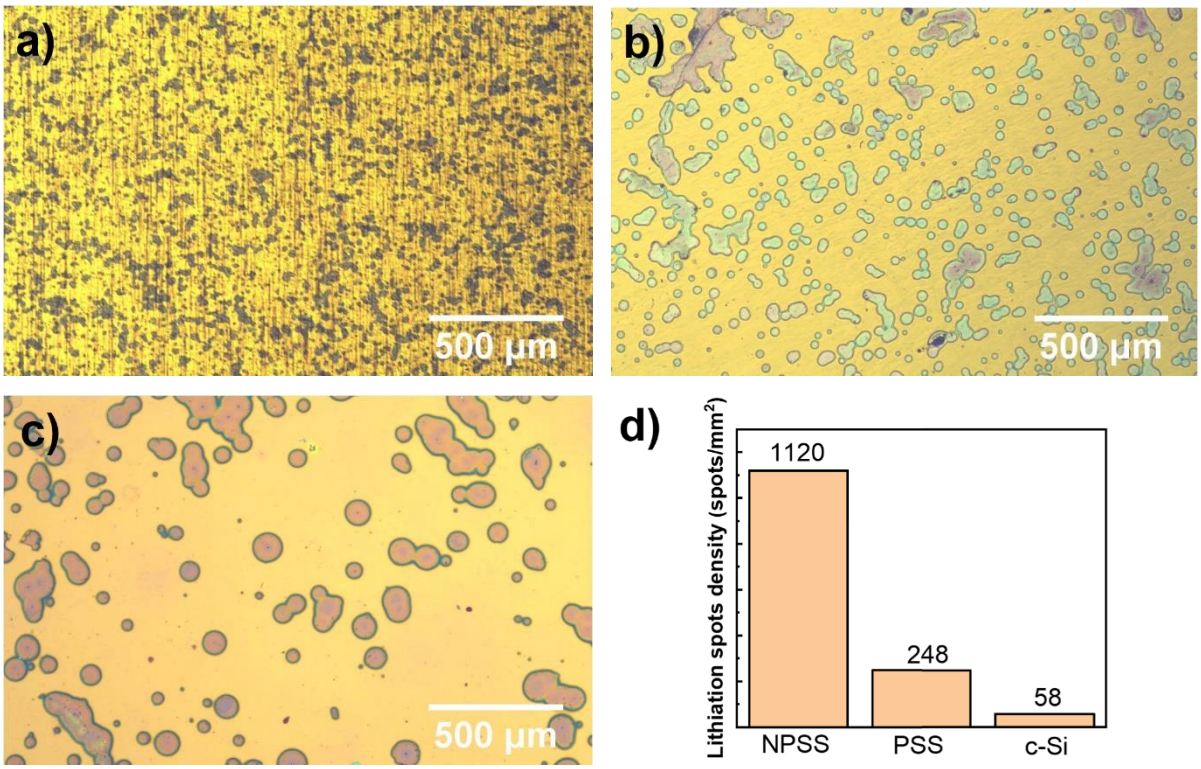

Figure 4. In-situ optical images of partially lithiated 10% methylated a-Si electrodes (100 nm thickness) deposited on different substrates: (a) non-polished stainless steel (NPSS), (b) electropolished stainless steel (PSS) and (c) electronic-grade crystalline silicon (c-Si). The vertical features distinguished on (a) are reminiscence of scratches existing on the surface of the NPSS substrate prior to the methylated a-Si layer deposition. Lithiation conditions: current density ~ 29 µA cm^{-2} corresponding to a C/2 lithiation rate, duration 12 min. (d) Density of lithiation spots on the three different substrates.

3.2. Existence of Ohmic Effects

In order to test for the existence of the postulated Ohmic effects, [39] experiments are performed at various current densities to study the impact of the electrochemical current on the lithiation homogeneity. Images of methylated a-Si electrodes (5% methyl content, 100 nm thick) after partial lithiation and using various charging rates are displayed in **Figure 5**. The current densities used for these experiments correspond approximately to C/15 (Figure 5a), C/2 (Figure 5b), and 200 C (Figure 5c) lithiation rates and the lithiation charge is approximately 10 µA h in all the experiments. The corresponding potential curves are shown in the right column. Color changes are observed in all cases, indicating that lithiation proceeds but that different behaviors are observed depending on the current density. At small lithiation rate (C/15, Figure 5a) a spatially uniform color change is observed from the onset of lithiation which is therefore uniform across the sample surface. As the lithiation rate is increased, the lithiation becomes inhomogeneous (Figure 5b-c). As for 10% methylated a-Si electrodes, the lithiation process starts at some specific locations giving rise to the formation of lithiated spots. At intermediate charging rate (C/2, Figure 5b) various sizes of lithiation spots are present on the surface, indicating their non-simultaneous nucleation. Non-homogeneous lithiation is still observed when further increasing the lithiation rate (200 C**,** Figure 5c). In this case the color mapping suggests the very fast nucleation of a large number of lithiation spots and their merging to form connected blue-green islands with purple edges. In both cases of non-homogeneous lithiation (samples b and c), for longer charging times the images show the lateral expansion of the blue-green areas until they fully cover the whole surface. The blue-green color observed inside the spots/islands for short time therefore corresponds to areas fully lithiated in depth.

Correlated to the observation of the non-uniform lithiation phenomenon, singular features are also evident on the potential curves. In the case of homogeneous lithiation the potential decreases gradually from the open-circuit potential (OCP) to a potential close to 280 mV

(Figure 5a). A different behavior is observed when the lithiation is not homogeneous. [39] A fast potential drop below the value of the potential plateau electrode (~ 200 mV) is systematically observed just after the electrode polarization. This over-potential drop is small for intermediate lithiation rates (Figure 5b) but much greater for high lithiation rates (Figure 5c). It is then clear that upon increasing the current, a larger potential drop is detected at the very early stage of the lithiation process, and remains sizeable at large current densities. This potential drop originates from the Ohmic drop associated with the current flowing through the poorly-conductive non-lithiated electrodes that act as a series resistance in the electrical circuit.

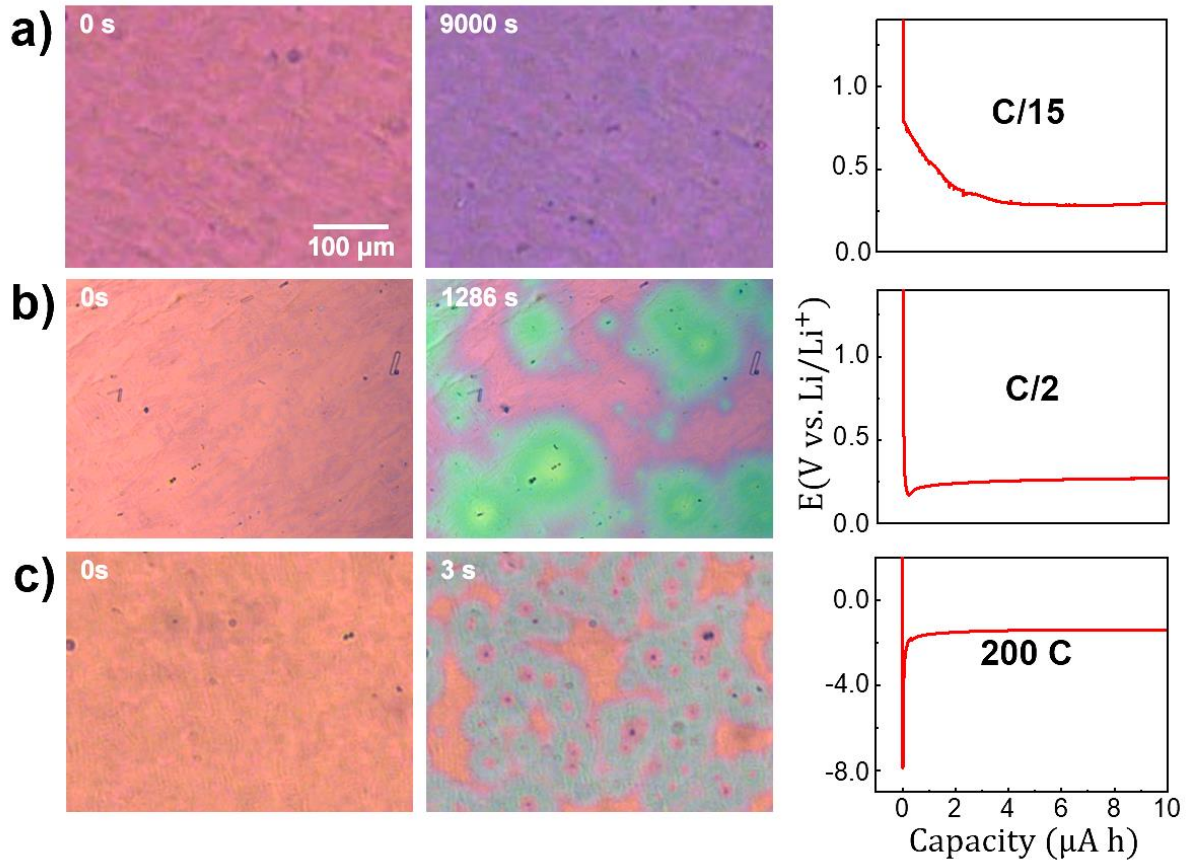

Figure 5. Left and middle columns: in-situ optical images of 5% methylated a-Si electrodes (100 nm thickness) before (left column) and after partial lithiation (middle column). Right column: Potential evolution at the beginning of the lithiation. Lithiation conditions: (a) current density ~ 4 µA cm^{-2} (C/15 lithiation rate), duration 9000 s (b) current density ~ 29 µA cm^{-2} (C/2 lithiation rate), duration 1286 s, (c) current density ~ 12600 µA cm^{-2} (200C lithiation rate), duration 3 s. Lithiation charge ~10 µA h for all samples.

The potential actually measured during the lithiation is given by the equation:

$$E_{measured} = E_W - \Delta E_{Ohmic} = E_W - IR \quad (1)$$

where the E_w is the potential of the a-Si electrode and ΔE_{ohmic} is the ohmic drop in the non-lithiathed part of the electrode (equal to the product of the electrochemical current by the ohmic resistance). Hence, the measured negative potential does not mean that the potential of the working electrode *vs* Li/Li^+ is negative. The high Ohmic resistance of the initial silicon layer implies the building-up of a possibly large negative voltage at the onset of the lithiation in the case of high current density. The fast decrease of the Ohmic drop at the very early stage of the lithiation sequence results from the appearance of more conductive areas (lithiation spots) that partially short-circuit the rest of the electrode.

For comparison, the effect of lithiation rate was also investigated in non-methylated a-Si electrodes. As for methylated material, a transition from homogeneous to inhomogeneous lithiation is observed when increasing the current density, but the transition is observed for a different current density (around a few 10C). Images of a-Si electrodes after partial lithiation at two different charging rates are displayed in **Figure 6**. In both cases the lithiation charge is approximately 7 µA h. As previously reported, [39] at a charging rate of C/2, lithiation is uniform whereas it is non-homogeneous for methylated a-Si. Figure 6b shows an electrode lithiated at 185 C (above the transition threshold) for 2.2 s. Here again the non-homogeneous lithiation phenomenon is associated with the observation of an over-potential drop at the very beginning of the lithiation, which does not exist in conditions of homogeneous lithiation (right column of Figure 6). Compared to methylated a-Si electrode, a higher current is needed to reach a non-uniform lithiation regime in non-methylated a-Si electrode. This is consistent with the

lower resistivity of non-methylated a-Si as compared to methylated a-Si material.

These results show that the lithiation can be tuned by adjusting the current density. In both methylated and non-methylated a-Si layers, increasing the lithiation current turns lithiation from uniform to non-uniform. Spatially uneven lithiation is always accompanied by a rapid drop in potential at the early lithiation stage. In the different materials, the magnitude of the current needed to switch from uniform lithiation to non-uniform lithiation is correlated to the resistivity of the pristine material. All these observations demonstrate that Ohmic effects drive the homogeneity of the lithiation of the considered silicon-based thin films.

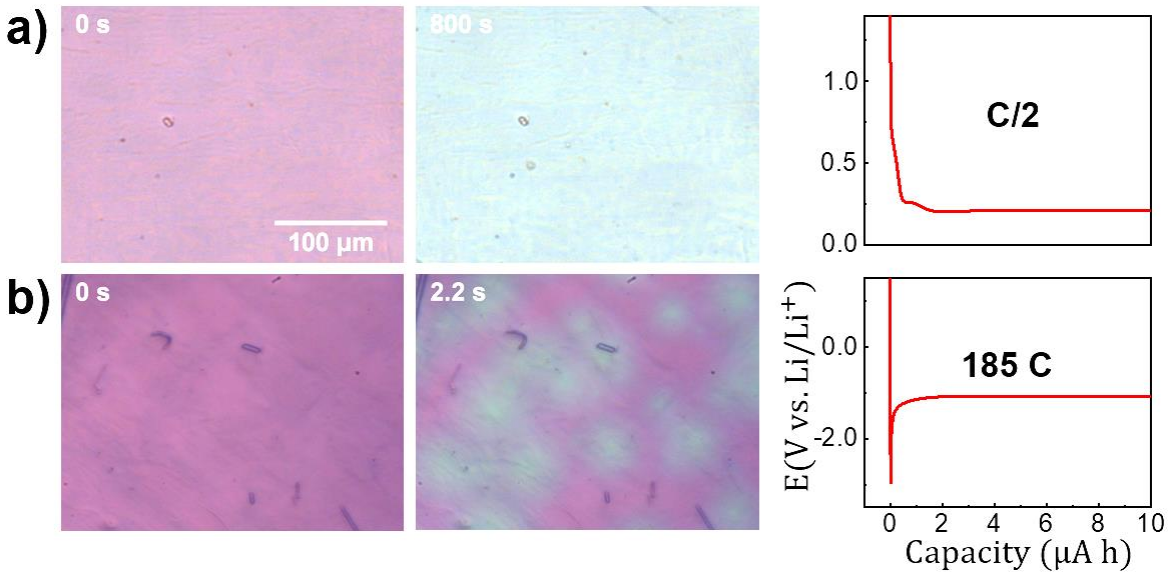

Figure 6. Left and middle columns: in-situ optical images of a-Si:H electrodes (100 nm thickness) before (left column) and after (middle column) partial lithiation. Right column: Potential evolution at the beginning of the lithiation. Lithiation conditions: (a) current density ~ 34 µA cm^{-2} (C/2 lithiation rate), duration 800 s, yielding a homogeneous lithiation; (b) current density ~ 12600 µA cm^{-2} (185C lithiation rate), duration 2.2 s. Lithiation charge ~7 µA h for both samples.

3.3. Doping of the material

A further assessment of the above conclusions, and a practical mean for circumventing the non-homogeneous character of the lithiation in (resistive) methylated amorphous silicon would be

to make this material more conductive. Therefore, measurements have been performed on boron-doped methylated layers, since boron is a usual dopant in silicon. The results obtained for 1% and 2% boron-doped electrodes are compared to those obtained for undoped electrodes in **Figure 7**. A same current density (~28 µA.cm^{-2}) is used for all samples, corresponding approximately to a C/2 lithiation rate. After partial lithiation (1000 s), the charge is 7.8 µA h.

In the initial state (Figure 7, left column), the color of the undoped electrode (a) is slightly different from the doped ones (b, c). It can be speculated that this may be due to a slight thickness difference or a minute change in the refractive index of the material induced by doping. After partial lithiation of the highly doped electrode the image shows a uniform color change from orange to purple (c). A spatially uniform lithiation of the whole surface is observed whereas under the same conditions the lithiation is non-uniform in the undoped electrode (a). Interestingly, for the intermediate doping (b), a combination of uniform and non-uniform lithiation process is observed: in addition to a quasi-uniform background color change (from orange to purple), blue-green spots can be distinguished that indicate the existence of preferential lithiation paths at some locations probably associated to low-resistance defects. For images recorded at longer times, a lateral expansion of these blue-green areas is observed until a uniform blue-green color is obtained, corresponding to full lithiation.

Correlated to the homogeneous lithiation process, the potential curves show a regular potential decrease. A small over-potential drop is observed (minimum value of around 182 mV) at the beginning of the lithiation in the case of the 1% doped electrode which is – here again – correlated to the observation of localized lithiation initiation.

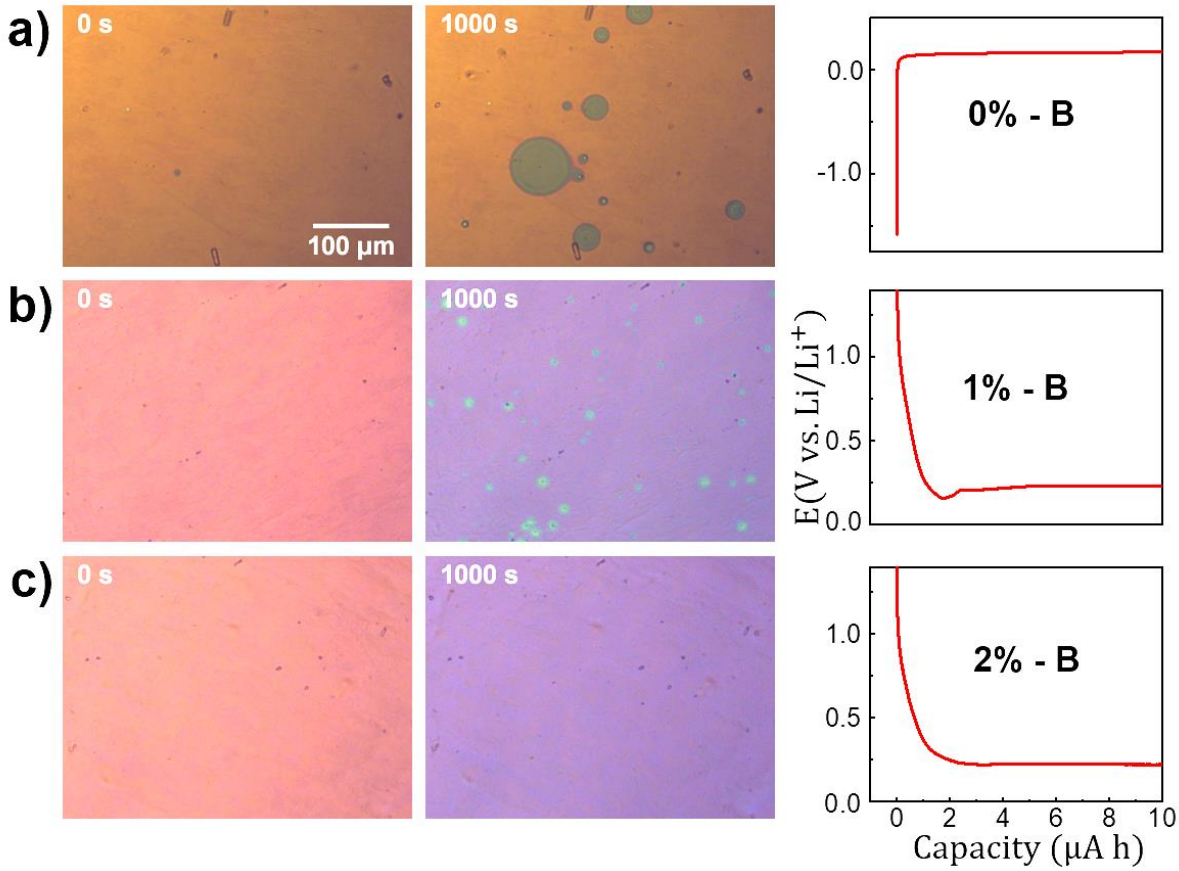

Figure 7. Left and middle columns: in-situ optical images of undoped (a), 1% (b) and 2% (c) boron-doped methylated a-Si electrodes (10% methyl content, 100 nm thick) electrolyte before (left column) and after partial lithiation (middle column). Right column: Potential evolution at the beginning of the lithiation. Lithiation conditions: current 28 µA cm^{-2} (C/2 lithiation rate), duration 1000 s.

Therefore, the first-lithiation behavior turns from inhomogeneous to homogeneous by increasing boron doping. In addition, as boron doping is increased, the magnitude of the initial potential drop decreases, which indicates that the layer resistance is effectively reduced by doping. Similar experiments have been attempted with phosphorus doping. Phosphorus is another usual dopant of silicon, but it turns out to be less efficient than boron for driving the homogeneity of the lithiation. This surprising result will be discussed in Section 4.2.

4. Discussion

The above results make clear that when the Ohmic drop through the active material is large enough, the first lithiation is spatially inhomogeneous and starts at some spots which then

expand and finally cover the whole surface. The origin of the spot nucleation and the factors driving the homogeneity of the first lithiation are now going to be discussed.

4.1. The nucleation of lithiation spots in the case of inhomogeneous lithiation

Defects are found at the center of these spots, as shown in Figure 2. Some of them are pre-existing, as shown in Figure 3: point locations at which the methylated amorphous silicon layer is thinner have been identified prior to lithiation and have been seen to possibly act as nucleation centers for lithiation spots. This observation is in line with the intuitive view that since these locations exhibit a lower electrical resistance, they are favoring the lithiation spot nucleation. However, as described in Section 3.1, it is also clear in Figure 3 that lithiation spots nucleate at locations where pre-existing defects have not been identified, especially at the very beginning of the lithiation, during the potential transient. It means that nucleation either takes place at not visible defects, or at defect-free locations. In this case, the initiation of the lithiation might proceed through a breakdown-like mechanism. Note that electric fields exceeding 100 kV cm^{-1} may appear at the very beginning of lithiation, supporting this possibility. Whatever the defect is pre-existing or induced by dielectric breakdown, one may infer that the very localized current flowing at the nucleation of the lithiation spot induces a local material degradation. This current-induced degradation is consistent with the observation that for a pre-existing defect identified prior to lithiation, the defect at the center of the lithiation spot appears much more clearly in the microscopic images after lithiation than prior to it, in agreement with the results presented in Figure 2.

Another conspicuous observation is that the nucleation of lithiation spots is time distributed. At the very beginning of the lithiation the spot nucleation seems associated with the electrical stress manifested by the existence of the potential transient; a lithiation spot then appears, either at an apparent defect-free location as in Figure 3, or at defects as observed in other experiments. At

subsequent times, the potential and the associated electric field across the methylated amorphous silicon layer decrease in magnitude but actually remain sizeable. The electric field therefore remains high enough for turning on still idle defects. The opening new conduction channels can take place through medium-field mechanisms that can inject electronic carriers across the semiconducting layer more progressively than dielectric breakdown [43], favoring the progressive nucleation of lithiation spots at locations where the electric field can better assist conduction. Intuitively, these locations are those where the electric field is larger, i.e., defects where the methylated a-Si layer is locally thinner. A closer look on the various pre-identified defects reveals that pinholes corresponding to a full perforation of the methylated a-Si layer do not act as efficient nuclei for lithiation spots, but that the pre-identified defects that correspond to the appearance of a lithiation spot are those which are the deepest without perforating the layer. In details, the times at which the nucleation spots appear do not totally map the value of the layer thickness at the corresponding defects (e.g., in Figure 3, the spot at defect 1 is starting before that at defect 2, whereas defect 2 appears slightly deeper than defect 1); in addition to the limits of confocal characterization, this observation can be accounted for by the fact that carrier injection in methylated a-Si will depend on both electric field and the presence and nature of electronic defects at the considered location. To summarize, the analysis of the evolution of lithiation spots in Figure 3 allows for distinguishing two nucleation mechanisms depending on the local electric field, as sketched in Figure 8a-b; some of the existing defects which experience a lower electric field, as sketched in Figure 8c, will not capture enough current for creating a lithiation spot before complete lithiation of the electrode surface.

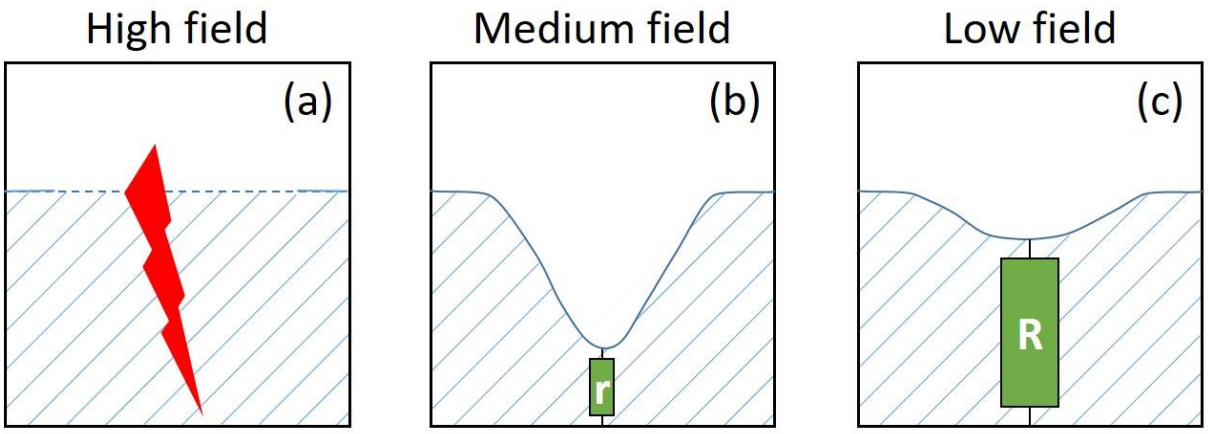

Figure 8. Schematics of the possible mechanisms for the nucleationn of lithiation spots. (a) During the initial potential transient, a high field is created, causing the instantaneous nucleation of a lithiation spot by dielectric breakdown, in the presence or in the absence of a defect; (b) At later stages, the medium electric field associated to a deep defect makes the local resistance weak enough for capturing a low current, initiating the progressive nucleation of a lithiation spot; (c) when a defect is too shallow, the electric field is too low and the resistance too high for nucleating a lithiation spot before the defect location is lithiated from the surrounding spots.

Independently from the origin of the spot nucleation (pre-existing defects or dielectric-breakdown-like phenomena), there appears to be a kind of competition for the nucleation of spots: when "large" defects (like scratches) are intentionally generated at the surface, nucleation preferentially starts at these location, at the expense of "natural" pre-existing defects (see **Figure S6**); in that case, no potential drop is observed as well as no spot induced by dielectric-breakdown. Conversely, the use of very high lithiation rates like in Figure 5c plausibly makes easier the nucleation of spots by dielectric breakdown.

In conclusion, when the first lithiation is inhomogeneous, the lithiation spots nucleate either progressively at pre-existing low-resistance defects, as previously suggested [39], or instantaneously under the influence of a high electric field, likely through a dielectric-breakdown mechanism. Whatever the origin of the nucleation is, the initial intense current density experienced at the initial stage of the spot formation induces a material degradation at the location of the nucleation. It generates a post-lithiation defect which is systematically found at the center of the lithiation spots.

4.2. Factors affecting the homogeneity of the first lithiation

A striking result described above is that acting on the lithiation rate can turn on or off the spatial inhomogeneity of the first lithiation of methylated amorphous silicon. High lithiation rate and high resistivity of the methylated amorphous silicon layer favor inhomogeneity of the first lithiation. On intuitive grounds, it appears clear that the lithiation front (separation between lihtiated and non lithiated phase) is intrinsically unstable in view of the resisting character of the non-lithiated phase. Once a lithiation spot is initiated, the reduced electrical resistance locally opposed to current flow will tend to focus all the current at this location (the "lightning rod" effect) and favor on-going lithiation at this location, making the lithiation spot expand first in the depth of the layer, and then laterally. This is a typical example of "Laplacian instability", i.e., a situation where an initially flat interface ruled by a Laplacian field, such as the electrostatic potential, develops specific patterns during its evolution. [44]

A powerful approach to quantitatively analyze such an instability is to perform a linear stability analysis, [45] an approach successfully used in the electrochemical context for investigating the formation of porous silicon [46-49] or porous anodic oxides. [50, 51] It allows for quantitatively studying the balance between stabilizing and destabilizing effects. In the present case, a linear stability analysis would require drastic approximations, since the system actually includes several interfaces, and yield results barely comparable with experimental observations since the thickness of the active layer is too thin for allowing the system to reach its steady-state configuration. We will therefore limit ourselves to a qualitative discussion of the instability.

The destabilizing effect of the electrical potential is described above. In addition, stabilizing effects are also contributing. The competition between stabilizing and destabilizing effect accounts for the observed change from homogeneous to inhomogeneous lithiation of a-Si:H when increasing the lithiation rate (see Figure 6). In the absence of stabilizing effects, a-Si:H, whose resistivity is expected to be larger than that of the lithiated phase, should undergo a non-

homogeneous lithiation. This is not observed at standard lithiation rates, at least at the timescale of the lithiation of the thin-film electrodes, which supports the presence of stabilizing effects. However, increasing the current (i.e., enhancing Ohmic effects and the destabilizing contribution of the electrical potential) modifies the balance between stabilizing and destabilizing effects and turn the lithiation inhomogeneous at the time scale of the experiments. Among possible stabilizing effects, one may invoke the reduced velocity of Li in the solid phase as compared to Li^+ ions in the electrolyte and the effect of compressive stresses extending into the lithiated phase and lowering the progression of the interface between lithiated and non-lithiated phases. [52] Similarly, increasing methyl concentration in the methylated a-Si increases the magnitude of the destabilizing effect since the material becomes more resistive. Conversely, doping methylated a-Si to make it more conductive decreases the destabilizing effect and turns the lithiation of methylated a-Si homogeneous, as shown in Figure 7.

In conclusion, the homogeneity of the lithiation of (methylated) a-Si appears to result from the competition between stabilizing and destabilizing effects. The most important destabilizing effects are related to Ohmic effects. They tend to favor the local growth of the conducting lithiated phase over the uniform lithiation of the resistive methylated a-Si layer. Acting on these effects by adjusting the lithiation current or changing the material resistivity modifies the balance between stabilizing and destabilizing effects and may switch the first lithiation of methylated a-Si between homogeneous and inhomogeneous.

4.3. Doping of Methylated Amorphous Silicon

The doping of methylated amorphous silicon also deserves a specific discussion (nature and concentration of the dopant). Boron has already been incorporated in Si anodes in the context of Li-ion batteries [22]. Most often, it has been used for making easier the elaboration of the material under porous or nanostructured form. The associated lowering of the Si resistivity is a

recognized consequence of Si doping; its impact on the lithiation performances appears weak for Si nanoparticles [53] but positive for Si-C composites [54]. Here, boron has been used for increasing the conductivity of methylated a-Si. For that purpose, at first sight, the dopant concentration (in the atomic percent range) appears quite high; however, substitutional doping efficiency is known to be poor in amorphous-silicon-based materials. [55, 56] This is due to the lower constraint of the covalent silicon network to force the doping impurities to adopt a tetravalent coordination as compared to crystalline silicon. As a consequence, high doping levels should be used as compared to those commonly used in crystalline silicon.

Another conspicuous observation is that boron is more efficient in making the methylated a-Si lithiation homogeneous than phosphorus, another commonly used doping impurity for making Si more conductive. Phosphorus doping of Si thin-film anodes has also been used in the context of Li-ion batteries; it has been reported to improve the electrode cycling performance better than boron doping [57]. Boron is a p-type dopant for silicon, whereas phosphorus is an n-type dopant. The more efficient boron effect on homogeneity, as compared to the phosphorus one, appears counterintuitive, since n-type impurities give free electrons to the semiconductor, whereas p-type impurities give free holes. In the reduction reaction of a Li^+ ion corresponding to the lithiation of the material, an electron (not a hole) is needed. As a matter of fact, lithiation is performed under strongly reducing conditions, at very low potentials (close to 0 V vs Li/Li^+). Under these conditions, at the semiconductor/electrolyte interface, the semiconductor bands are bent strongly downwards as schematically shown in **Figure 9**. The electrode potential (corresponding to the position of the Fermi level in the semiconductor) is slightly positive relative to that of the Li/Li^+ redox couple, which corresponds to a position of the Fermi level in the bulk semiconductor slightly below the energy level associated with the Li/Li^+ redox couple (see Figure 8). Therefore, the relevant states for transferring an electron to electrolyte species are those of the conduction band for P-doped (n-type) methylated amorphous silicon, but those

of the valence band, with a tunnel mechanism across the thin space-charge region at the semiconductor surface, for B-doped (p-type) methylated amorphous silicon. This difference is pointed out by the horizontal arrows in Figure 9. Even though the overlap of the (solvation broadened) Li/Li^+ energy level with conduction-band states is more favorable for the P-doped material than that with valence-band states for the B-doped material, the situation is more than compensated by the order-of-magnitude difference in the occupation of the corresponding electronic states in the semiconductor (nearly empty in the conduction band, fully occupied in the valence band). This situation makes the electron transfer much easier in the case of the B-doped material as compared to the P-doped one, which decreases the effective resistance at the semiconductor/electrolyte interface.

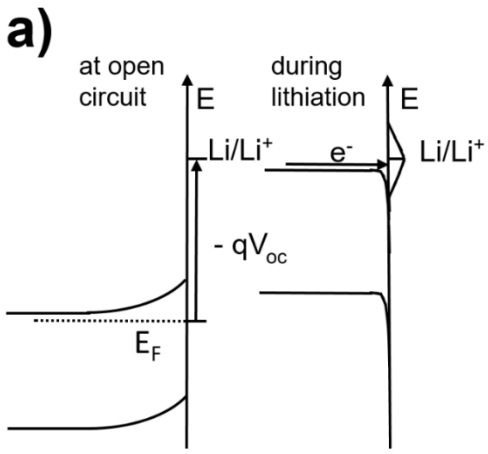

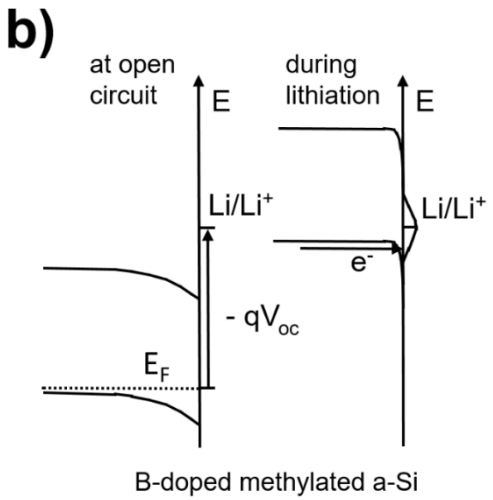

Figure 9. Energy-band diagrams of phosphorus- and boron-doped methylated a-Si, at open circuit and during lithiation process. This scheme does not take into account the disorder effects in amorphous semiconductors (presence of band tails, sizeable density of states associated with deep localized states) but only retains the general features of a semiconductor/electrolyte interface. [58]

5. Conclusion

Spatially homogeneous or inhomogeneous lithiation processes are observed by operando optical microscopy both on pure a-Si and methylated a-Si thin layers during their first lithiation. Inhomogeneous lithiation is observed at low lithiation rate in methylated a-Si, whereas it appears at higher lithiation rate in pure a-Si. An electrostatic instability associated with the resistive character of the material is found to be responsible for the observation of the lithiation spots and inhomogeneous lithiation. Experimental observations reveal the existence of defects that act as nucleation centers for the lithiation spots. These defects are in some cases pre-existing morphological defects in the layer, or in other cases appear to be created by the large current flowing at the locations where the instability triggers a lithiation-spot nucleation.

Doping gives a practical means for turning the first lithiation homogeneous. The first-lithiation behavior turns from inhomogeneous to homogeneous by increasing boron-doping from 0% to 2% in 10% methylated a-Si electrodes. Doping may also give practical access to higher methyl

concentrations which should present practical advantages for the electrochemical cycling of these highly resistive materials [25].

Acknowledgements
Délégation Générale de l'Armement (DGA) is gratefully acknowledged for financial support. This work has also been supported by a public grant overseen by the French National Research Agency (ANR) as part of the "Investissements d'Avenir" program (Labex Charmmmat, ANR-11-LABX-0039-grant). It was produced within the framework of Energy4Climate Interdisciplinary Center (E4C) of IP Paris and Ecole des Ponts ParisTech.

References

[1] J. Lu, Z.W. Chen, F. Pan, Y. Cui, K. Amine, Electrochem. Energy Rev., 1 (2018) 35-53.

[2] X. Zuo, J. Zhu, P. Müller-Buschbaum, Y.-J. Cheng, Nano Energy, 31 (2017) 113-143.

[3] F. Ozanam, M. Rosso, Materials Science and Engineering: B, 213 (2016) 2-11.

[4] X. Zhao, V.-P. Lehto, Nanotechnology, 32 (2020) 042002.

[5] M. Ashuri, Q. He, L.L. Shaw, Nanoscale, 8 (2016) 74-103.

[6] U. Kasavajjula, C.S. Wang, A.J. Appleby, Journal of Power Sources, 163 (2007) 1003-1039.

[7] C.K. Chan, H.L. Peng, G. Liu, K. McIlwrath, X.F. Zhang, R.A. Huggins, Y. Cui, Nature nanotechnology, 3 (2008) 31-35.

[8] M.H. Park, M.G. Kim, J. Joo, K. Kim, J. Kim, S. Ahn, Y. Cui, J. Cho, Nano letters, 9 (2009) 3844-3847.

[9] N. Liu, H. Wu, M.T. McDowell, Y. Yao, C. Wang, Y. Cui, Nano letters, 12 (2012) 3315-3321.

[10] M.T. McDowell, S.W. Lee, W.D. Nix, Y. Cui, Advanced Materials, 25 (2013) 4966-4985.

[11] H. Wu, G. Chan, J.W. Choi, I. Ryu, Y. Yao, M.T. McDowell, S.W. Lee, A. Jackson, Y. Yang, L. Hu, Y. Cui, Nature nanotechnology, 7 (2012) 310-315.

[12] N. Liu, Z.D. Lu, J. Zhao, M.T. McDowell, H.W. Lee, W.T. Zhao, Y. Cui, Nature nanotechnology, 9 (2014) 187-192.

[13] W.L. An, B.A. Gao, S.X. Mei, B. Xiang, J.J. Fu, L. Wang, Q.B. Zhang, P.K. Chu, K.F. Huo, Nat. Commun., 10 (2019).

[14] H. Jia, J. Zheng, J. Song, L. Luo, R. Yi, L. Estevez, W. Zhao, R. Patel, X. Li, J.-G. Zhang, Nano Energy, 50 (2018) 589-597.

[15] F. Wu, J. Maier, Y. Yu, Chemical Society Reviews, 49 (2020) 1569-1614.

[16] J.T. Yin, M. Wada, K. Yamamoto, Y. Kitano, S. Tanase, T. Sakai, Journal of the Electrochemical Society, 153 (2006) A472-A477.

[17] S. Bourderau, T. Brousse, D.M. Schleich, Journal of Power Sources, 81-82 (1999) 233-236.

[18] S.K. Soni, B.W. Sheldon, X. Xiao, A. Tokranov, Scripta Materialia, 64 (2011) 307-310.

[19] S. Ohara, J. Suzuki, K. Sekine, T. Takamura, Journal of power sources, 136 (2004) 303-306.

[20] A. Mukanova, A. Jetybayeva, S.-T. Myung, S.-S. Kim, Z. Bakenov, Materials Today Energy, 9 (2018) 49-66.

[21] M. Salah, P. Murphy, C. Hall, C. Francis, R. Kerr, M. Fabretto, Journal of Power Sources, 414 (2019) 48-67.

[22] M. Salah, C. Hall, P. Murphy, C. Francis, R. Kerr, B. Stoehr, S. Rudd, M. Fabretto, Journal of Power Sources, 506 (2021) 230194.

[23] J. Li, A.K. Dozier, Y. Li, F. Yang, Y.-T. Cheng, Journal of The Electrochemical Society, 158 (2011) A689.

[24] H.B. Chew, B. Hou, X. Wang, S. Xia, International Journal of Solids and Structures, 51 (2014) 4176-4187.

[25] L. Touahir, A. Cheriet, D.A. Dalla Corte, J.-N. Chazalviel, C. Henry de Villeneuve, F. Ozanam, I. Solomon, A. Keffous, N. Gabouze, M. Rosso, Journal of Power Sources, 240 (2013) 551-557.

[26] I. Solomon, M.P. Schmidt, H. Tran-Quoc, Physical review. B, Condensed matter, 38 (1988) 9895-9901.

[27] I. Solomon, M.P. Schmidt, C. Sénémaud, M. Driss Khodja, Physical Review B, 38 (1988) 13263-13270.

[28] C. Cao, H.-G. Steinrück, B. Shyam, M.F. Toney, Advanced Materials Interfaces, 4 (2017) 1700771.

[29] B.M. Koo, D.A.D. Corte, J.-N. Chazalviel, F. Maroun, M. Rosso, F. Ozanam, Advanced Energy Materials, 8 (2018) 1702568.

[30] M.N. Obrovac, L. Christensen, Electrochemical and Solid-State Letters, 7 (2004) A93.

[31] J.M. Paz-Garcia, O.O. Taiwo, E. Tudisco, D.P. Finegan, P.R. Shearing, D.J.L. Brett, S.A. Hall, Journal of Power Sources, 320 (2016) 196-203.

[32] P. Limthongkul, Y.-I. Jang, N.J. Dudney, Y.-M. Chiang, Acta Materialia, 51 (2003) 1103-1113.

[33] D. Alves Dalla Corte, G. Caillon, C. Jordy, J.-N. Chazalviel, M. Rosso, F. Ozanam, Advanced Energy Materials, 6 (2016) 1501768.

[34] M.J. Chon, V.A. Sethuraman, A. McCormick, V. Srinivasan, P.R. Guduru, Physical Review Letters, 107 (2011) 045503.

[35] X.H. Liu, J.W. Wang, S. Huang, F. Fan, X. Huang, Y. Liu, S. Krylyuk, J. Yoo, S.A. Dayeh, A.V. Davydov, Nature nanotechnology, 7 (2012) 749-756.

[36] J.W. Wang, Y. He, F. Fan, X.H. Liu, S. Xia, Y. Liu, C.T. Harris, H. Li, J.Y. Huang, S.X. Mao, T. Zhu, Nano letters, 13 (2013) 709-715.

[37] M.T. McDowell, S.W. Lee, J.T. Harris, B.A. Korgel, C. Wang, W.D. Nix, Y. Cui, Nano letters, 13 (2013) 758-764.

[38] J. Li, J. Dahn, Journal of The Electrochemical Society, 154 (2007) A156.

[39] Y. Feng, T.D.T. Ngo, M. Panagopoulou, A. Cheriet, B.M. Koo, C. Henry-de-Villeneuve, M. Rosso, F. Ozanam, Electrochimica Acta, 302 (2019) 249-258.

[40] I. Solomon, R. Benferhat, H.T. Quoc, Physical Review B, 30 (1984) 3422.

[41] M. Bhatnagar and I. Solomon, unpublished results

[42] M. Bhatanagar, PhD thesis 1992, University Paris 6

[43] J. Chévrier, B. Equer, Journal of applied physics, 76 (1994) 7415-7422.

[44] P. Garik, D. Barkey, E. Ben-Jacob, E. Bochner, N. Broxholm, B. Miller, B. Orr, R. Zamir, Physical Review Letters, 62 (1989) 2703-2706.

[45] W.W. Mullins, R.F. Sekerka, Journal of Applied Physics, 35 (1964) 444-451.

[46] Y. Kang, J. Jorné, Journal of The Electrochemical Society, 140 (1993) 2258-2265.

[47] Y. Kang, J. Jorné, Journal of The Electrochemical Society, 144 (1997) 3104-3111.

[48] R.B. Wehrspohn, F. Ozanam, J.N. Chazalviel, Journal of The Electrochemical Society, 146 (1999) 3309-3314.

[49] J.N. Chazalviel, R.B. Wehrspohn, F. Ozanam, Materials Science and Engineering: B, 69-70 (2000) 1-10.

[50] G.K. Singh, A.A. Golovin, I.S. Aranson, Physical Review B, 73 (2006) 205422.

[51] K.R. Hebert, S.P. Albu, I. Paramasivam, P. Schmuki, Nature materials, 11 (2012) 162-166.

[52] S. Zhang, npj Computational Materials, 3 (2017) 7.

[53] S. Rousselot, M. Gauthier, D. Mazouzi, B. Lestriez, D. Guyomard, L. Roue, JOURNAL OF POWER SOURCES, 202 (2012) 262-268.

[54] R. Yi, J.T. Zai, F. Dai, M.L. Gordin, D.H. Wang, ELECTROCHEMISTRY COMMUNICATIONS, 36 (2013) 29-32.

[55] W.E. Spear, P.G. Le Comber, Solid State Communications, 17 (1975) 1193-1196.

[56] M. Stutzmann, D.K. Biegelsen, R.A. Street, Physical Review B, 35 (1987) 5666-5701.

[57] A. Mukanova, A. Serikkazyyeva, A. Nurpeissova, S.-S. Kim, M. Myronov, Z. Bakenov, Electrochimica Acta, 330 (2020) 135179.

[58] H. O. Finklea, in Semiconductor Electrodes, H. O. Finklea (ed.), Elsevier, Amsterdam 1988, pp. 1-42.